Atmos. Chem. Phys. Discuss., 11, 567–595, 2011
www.atmos-chem-phys-discuss.net/11/567/2011/
doi:10.5194/acpd-11-567-2011

Atmospheric Chemistry and Physics Discussions

Scavenging of biomass burning refractory black carbon and ice nuclei in a Western Pacific extratropical storm

J. L. Stith[1], C. H. Twohy[2], P. J. DeMott[3], D. Baumgardner[4], T. Campos[1], R.-S. Gao[5], and J. Anderson[6]

[1]National Center for Atmospheric Research, Boulder, Colorado, USA
[2]College of Oceanic and Atmospheric Sciences, Oregon State University, Corvallis, Oregon, USA
[3]Department of Atmospheric Sciences, Colorado State University, Fort Collins, Colorado, USA
[4]Centro de Ciencias de la Atmósfera, Universidad Nacional Autónoma de México, Mexico City, Mexico
[5]Chemical Sciences Division, NOAA Earth System Research Laboratory, Boulder, Colorado, USA
[6]Mechanical and Aerospace Engineering, Arizona State University, Tempe, Arizona, USA

Received: 16 December 2010 – Accepted: 16 December 2010 – Published: 7 January 2011

Correspondence to: J. L. Stith (stith@ucar.edu)

Published by Copernicus Publications on behalf of the European Geosciences Union.

Abstract

In situ airborne sampling of refractory black carbon (rBC) particles and Ice Nuclei (IN) was conducted in and near an extratropical cyclonic storm in the Western Pacific Ocean during the Pacific Dust Experiment, PACDEX, in the spring of 2007. Airmass origins were from Eastern Asia. Cloud hydrometeors were evaporated by a counterflow virtual impactor and the residue was sampled by a single particle soot photometer (SP2) instrument and a continuous flow diffusion chamber ice nucleus detector. Clouds associated primarily with the warm sector of the storm were sampled at various locations and altitudes. In storm midlevels at temperatures where heterogeneous freezing is expected to be significant (here −24 to −29°C), IN measurements from ice particle residues generally agreed well with simultaneous measurements of total ice concentrations provided that the measurements were made at ambient temperatures similar to those in the CFDC chamber, suggesting heterogeneous freezing as the dominant ice formation process in the mid levels of these warm sector clouds. Lower in the storm, at warmer temperatures (−22 to −6.4°C), ice particle concentrations were similar to IN concentrations at CFDC chamber temperatures representative of colder temperatures. This is consistent with ice particles forming at storm mid-levels by heterogeneous freezing on IN, followed by sedimentation to lower altitudes. Homogeneous freezing did not appear to contribute significantly to midlevel ice concentrations and rime-splintering was also unlikely due to the absence of significant supercooled liquid water in the warm sector clouds. IN number concentrations were typically about a factor of five to ten lower than simultaneous measurements of rBC concentrations in cloud.

1 Introduction

Black carbon (BC) aerosols are of fundamental interest to studies of anthropogenic climate change because of their ability to absorb sunlight and the fact that they have a large anthropogenic source through direct emissions from fossil fuels or indirectly

ACPD
11, 567–595, 2011

through anthropogenic influences on biomass burning. Aerosols containing soot and other forms of BC aerosols have been implicated in reducing tropical cloudiness (Ackerman et al., 2000), in changing precipitation and temperature patterns (Menon et al., 2002), and have been suggested to be the strongest contributor to global warming after carbon dioxide (Ramanathan and Carmichael, 2008). Trans-Pacific transport of BC from Asia is thought to impact radiative forcing as far away as North America (Hadley et al., 2007).

The interaction of BC with clouds is of particular interest, because clouds and precipitation provide a major removal mechanism for BC and because BC containing particles may alter the microphysical structure of clouds by acting as cloud condensation nuclei (CCN) or as ice forming nuclei (IN). The inclusion of BC in liquid or ice particles may also influence the climate impact of clouds (e.g., Jacobson, 2006) by changing their radiative properties.

In spite of the importance of the interactions of BC with clouds, there are relatively few observations that demonstrate its major pathways for incorporation into clouds. Some BC may be incorporated into clouds through nucleation, with BC acting as either CCN or IN. For example, Cozic et al. (2008) observed enrichment in the BC aerosol mass fraction in ice particle residue, compared to the mass fraction outside of cloud. They suggested that this result might be due to BC-containing particles acting preferentially as IN. However, Baumgardner et al. (2008) studied Northern Pacific cirrus cloud residuals and concluded that inertial scavenging was likely to be more important than nucleation for scavenging BC. A number of other aerosol particles are thought to serve as IN, such as dust particles, which are abundant from Asian sources (e.g., see Stith et al., 2009 and references therein).

Understanding the origins of ice in storms and the relationship between ice in the clouds and aerosols continues to be a fundamental problem in cloud physics. This is especially important for understanding the possible effects of anthropogenic aerosols on storms and their climatologically significant properties, such as precipitation, storm/cloud lifetimes and cloud optical properties. Dusts such as those from Asia

ACPD
11, 567–595, 2011

or Africa are known to be a source of both IN and CCN, but their impact on storms is not well known. Part of this difficulty is that ice-containing clouds in deep storms probably contain ice from several sources, including homogenous freezing, heterogeneous freezing (via IN), and by secondary production, such as by Hallett-Mossop rime-splintering. In order to experimentally study the relationship between IN and ice in storms the sampling needs to be isolated to regions where heterogeneous freezing is likely to be active and where the ice in the storm is not contaminated by the other ice-creating mechanisms. Of course, at a given time and sampling location only one ambient temperature and one CFDC chamber temperature is measured, while the actual ice particle that are measured at that location could have formed at colder temperatures and fallen to the sampling location (or they could have even warmer regions if there are significant updrafts that carried the particles to the sampling location, although significant updrafts were not generally found in the areas we sampled). We often used a CFDC sampling temperature set near ambient for constant-altitude passes through the clouds, so that the numbers of IN measured should best correspond to ice particles forming nearby and are likely a lower limit for concentrations of particles that might have formed at colder temperatures in the same airmass that were at the sampling location due to sedimentation (neglecting the process of aggregation).

In this paper we examine refractory BC (rBC) and IN in residuals from cloud droplets and ice particles from a large extratropical spring storm in the Western North Pacific Ocean. Carbon Monoxide (CO) measurements indicated the presence of pollution from East Asia in the storm. Extensive airborne sampling of both warm and cold clouds associated with the warm front was conducted. In this part of the storm, Hallett-Mossop secondary ice production was not likely, which allowed relatively uncontaminated comparison between IN and measured ice concentrations. The measurements available from the project included single particle counting of refractory rBC particles which, even in relatively clean conditions, provides concentrations on approximately 10 s time scales and allows us to evaluate the scavenging properties of clouds over distances of about 2 km. Concurrent IN measurements were available and processed for 60 s time

ACPD
11, 567–595, 2011

scales (~12 km) so that we can examine the association between IN, rBC and other aerosol particles at a relatively high spatial resolution compared to the synoptic regions of the storm.

2 Venue and instrumentation

The storm was one of the cases from the Pacific Dust Experiment (PACDEX) during which a series of fourteen research flights were conducted in the April/May 2007 time period to sample pollution and dust outbreaks from East Asia as they interacted with Northern Pacific storms. The experiment, instrumentation, and early results from the project have been described in detail by Stith et al. (2009), so only a brief overview will be provided here.

PACDEX utilized the NSF/NCAR G-V aircraft, to carry a variety of instruments for aerosol and cloud physics measurements. A titanium Counterflow Virtual Impactor (CVI) mounted on the bottom of the G-V fuselage was used to sample cloud particles above the CVI threshold size of about 5 µm aerodynamic diameter. It provided measurements of condensed water content and a stream of the evaporated residual particles for further analyses and characterization by other instruments. The subisokinetic nature of the CVI provides for an enhancement by approximately a factor of 25 for the residual particles. This allows for improved statistics for low number concentration particles, such as IN. A HIAPER modular inlet (see Stith et al., 2009 for more information on this inlet) was used outside of cloud to sample aerosols and trace gases. Particles were collected for scanning and transmission electron microscopy using the procedures described in Stith et al. (2009).

Particles containing rBC were sampled by a Droplet Measurement Technologies (DMT) single particle soot photometer (SP-2). It measures the refractory component of BC mass and number by laser induced incandescence and particle size by light scattering in the range of 0.08 to 0.3 µm for rBC mass equivalent diameter; however, particles above about 0.19 µm saturate the detector and are counted, but are not sized.

ACPD
11, 567–595, 2011

Particles that are counted are also used to determine a total scattered particle concentration, which is useful to determine the relative fraction of rBC to total particles counted by the SP2 instrument. (Particles can also be sized by reference to their optical diameter rather than their mass equivalent diameter).

IN measurements were made with a continuous-flow (ice-thermal) diffusion chamber (CFDC), which, for the case presented in this paper, was operated at near and just above water saturation to favor a combination of ice freezing mechanisms, but especially condensation/immersion freezing (see DeMott et al., 2010 for more details). Based on the discussion in Prenni et al. (2009), we estimate the counting uncertainty associated with a 60 s running mean while sampling from the CVI (with its associated enhancement factor) to be approximately 0.1 per liter for concentrations of 1 per liter. The CFDC was fitted with an impactor for collecting the ice crystals formed from activated IN onto electron microscopy grids for post-analysis.

Other PACDEX instruments used in this study included a modified high speed 64-element Particle Measuring Systems (PMS)-based OAP-2DC optical array instrument (2DC), a DMT Ultra-High Sensitivity Aerosol Spectrometer (UHSAS) used here to measure aerosols between 0.1 and 1.0 µm, a fast-response dual-column continuous-flow streamwise thermal gradient CCN chamber, a DMT Cloud Droplet Probe (CDP) to measure cloud droplets and aerosols 2–50 µm in diameter, a vacuum UV absorption analyzer for CO (with precision of 3 ppbv for a 1 Hz sample rate), and a dual-beam UV-absorption ozone photometer (precision of approximately 1 ppbv at 200 hPa). Further details on these and the other PACDEX airborne instruments, including references, are provided in Stith et al. (2009).

The 2DC is used here to sample particles that image three or more of the 25 micron diodes (particles greater than about 75 microns). Smaller images are excluded to reduce uncertainties associated with their depth of field. (The CDP provides a qualitative measure of this smaller particle mode for quasi-spherical ice, however). Processing of the 2DC imagery to produce hydrometeor concentrations required particles to be inside the optical array (which is sometimes referred to as the "everything in" method) to

ACPD
11, 567–595, 2011

be counted and included an artifact rejection criteria for images that were over 4 times longer in the direction of flight than in the perpendicular direction (to avoid "streaker" type artifacts). Data presented here represent 10 s averages, unless otherwise indicated.

3 Storm characteristics and flight procedures

The storm was sampled on 17 May 2007. It exhibited a classic cold and warm frontal structure that was evident in the satellite image (Fig. 1). The storm region was examined for over 8 h with the G-V, including several descents and ascents to obtain vertical profiles through the cloud and clear air regions and horizontal transects, which were focused primarily on the warm frontal clouds/warm sector (above the warm frontal surface aloft) air and the cool sector (below the warm frontal surface aloft). In situ identification of the location of the warm frontal region was made by examination of the wind shift and temperature changes consistent with passage through a warm front.

An example of one vertical profile that was taken primarily near the southeastern edge of the storm is provided in Fig. 2. The profile was outside of most of the clouds, except for some thin cirrus in the upper portion of the profile. A clear demarcation in chemical airmass characteristics is evident at the location of the warm front. The properties of the warm sector airmass are unusual because the concentrations of CO (nearly 200 ppbv in Fig. 2 top) suggests a polluted airmass, yet the levels of ozone (Fig. 2 bottom) and the concentration of aerosols 0.1 to 1.0 µm and rBC (Fig. 2 top and middle) indicates that the warm sector airmass was rather clean in terms of aerosol and ozone. Examination of particles 0.5 to 1.0 microns in size (not shown), which we use as an indicator of dust, decreased to less than 0.01 cm^{-3} in the warm sector profile in Fig. 2. A likely explanation for these somewhat contradictory results is seen by examining the history of the warm sector and cool sector airmasses. Figure 3 provides a back-trajectory analysis from the NOAA HYSPLIT model (Draxler and Rolph, 2010) for locations in the warm and cool sector airmasses. Figure 4 provides the

ACPD
11, 567–595, 2011

corresponding model predicted rainfall history. The model suggests that each trajectory passed over different possible pollution sources in East Asia and the warm sector air had more encounters with precipitation than the cool sector air. Thus enhanced scavenging of aerosol particles and ozone precursors seems to be a likely explanation for the somewhat unusual characteristics of the warm sector air, in addition to possible differences in source origin. Extensive biomass burning was present in the source region for the warm sector air (Fig. 3, bottom), suggesting a likely biomass burning source for the rBC and some of the other particles that were sampled in the storm. The biomass burning source was confirmed by chemical analysis of particles (see below).

4 IN and BC in the upper warm-sector clouds

Simultaneous IN and rBC measurements of CVI residuals are available from a long horizontal transect through the storm at 8.5 km altitude (Fig. 1 long black track) and at ambient temperatures between −24 and −29 °C. A comparison of the IN concentrations measured from CVI cloud residual particles in the CFDC in the cabin of the aircraft with the ice concentrations measured by the 2DC instrument on the wing is shown in Fig. 5 (liquid water was not found on this pass). The transect was mostly in the warm sector cloud except after 05:57 UT, when the upper level front was encountered and the air mass changed from warm sector to cool sector (at the arrow in the lower part of Fig. 5). During this pass the CFDC was operated near water saturation and held at a temperature similar to ambient. The rather good agreement between IN concentrations and ice particle measurement is noteworthy, given the difficulties in correlating ice particles with IN, even in relatively simple clouds such as wave clouds (e.g., Eidhammer et al., 2010). Examination of the 2DC images (Fig. 6, top) revealed that most ice particles were a few hundred μm in size and, although there were some small ice images (close to 75 μm in size), they were rather few in number. During this pass the CDP concentrations were much lower than the 2DC concentrations (Fig. 6, bottom), also suggesting the absence of a small particle ice particle mode for this case.

ACPD
11, 567–595, 2011

Ice images included bullet rosettes, columns and possibly combinations of side planes, bullets and columns. The form of the ice particle was often obscured by either sideplane growth or feathery growth, but did not exhibit rounded edges that might indicate extensive riming (which is consistent with the lack of supercooled liquid water). These types of ice crystals are consistent with growth occurring at temperatures near these sampling temperatures. This particular region of the cloud, with well developed single ice crystals, likely grown by vapor deposition to a few hundred microns in size are good candidates for comparison with the CFDC measurements, because they are of a size easily sampled by the 2DC. The observation that the numbers of ice crystals correspond to the number of ice nuclei further suggests freezing occurred at similar temperatures to those in the CFDC.

While we attempted to operate the CFDC at temperatures close to the temperature of the ambient air, deviations, particularly near the start and end of the run, occurred due to changes in ambient conditions and drift in the chamber control. The observed differences between the IN concentrations and the 2DC concentrations were roughly in line with expected IN behavior with changes in temperature and are evident in the beginning and end of the pass (Fig. 5, bottom). When the CFDC chamber was significantly colder than ambient, more IN were measured than ice particles and when the CFDC chamber was warmer than ambient fewer IN than ice particles were observed. It is also evident that the results are not symmetrical with respect to temperature (e.g. a positive temperature difference does not carry the same impact as a negative temperature anomaly). In DeMott et al. (2010) a 3° temperature change equates to at most a change in IN concentration of about a factor of 2 for the same aerosol loading. The results in Fig. 5 suggest a stronger change; however, the aerosol properties in this case may differ significantly from the average conditions studied by DeMott et al. (2010).

Large ice crystals are likely to breakup during collection inside the CVI due to inertial stresses when impacting within the slowly moving counterflow region. Crystal breakup (or "shattering") has been shown to affect a variety of cloud physics measurements; see Jensen et al. (2009) for an overview. Large drops have also been shown

ACPD
11, 567–595, 2011

to produce enhanced concentrations of residual particles during high-speed sampling (Weber et al., 1998; Twohy et al., 2003). Based on the ratio of drag stress to surface energy density (e.g., Schwarzenböck and Heintzenberg, 2000), the threshold breakup size for quasi-spherical ice is expected to be about 70 µm diameter under the sampling conditions for this case (airspeed of 200 m s^{-1}, pressure of 345 hPa, bulk ice surface energy of 120 g s^{-2}). This corresponds to a Weber number of about 10, where water droplets have been observed to breakup (Pilch and Erdman, 1987; Tarnogrodzki, 1993). Slightly smaller droplet or crystals may survive the virtual impaction at the CVI probe tip, but fragment when they reach the bend where the sample flow is brought into the aircraft (Anderson and Twohy, 1993).

Multiple ice fragments from a single ice crystal could produce a significantly larger number of residual aerosol particles than ice particles if each crystal contains non-volatile material other than a single solid nucleus. Processes by which this could occur include freezing of large drops containing solute or inclusions distributed throughout their volume, scavenging of interstitial aerosol particles, or even chemical reactions occurring preferentially on the ice surface (Chen and Crutzen, 1994). SP2 rBC and total particle concentrations were measured in the CVI sample stream simultaneously with the IN. rBC concentrations in ice particle residue were substantially higher (by a factor of about 5 to 10) than either the IN or the 2DC ice concentrations, and the total number of particles seen by the SP2 was even greater (Fig. 7). This suggests that each ice particle contained multiple aerosol particles, including rBC, compared to the number of IN in the particles. Examination of the number of aerosol particles (IN, SP2 total scattering, and rBC) versus the condensed water content suggests that the number of aerosol particles released upon evaporation is well correlated with the condensed water content in the ice phase (Fig. 7, bottom) for each class of aerosol. The observation that there are more IN than ice particles at CFDC temperatures colder than ambient is consistent with the production of multiple aerosol particles upon evaporation/breakup of ice in the CVI; some of these particles apparently act as IN at colder temperatures. Scavenging rates of aerosol particles by ice crystals were estimated based on

ACPD
11, 567–595, 2011

Miller and Wang (1978), who include gravitational, inertial, thermophoretic and diffusiophoretic processes. Scavenging rates are dependent on a number of factors and are highest for particles smaller than 100 nm, where Brownian diffusion dominates. However, scavenging is still significant for particles 100 nm and larger and can be as high as a few particles per cm^{-3} per crystal per hour. Electrical effects, if present, can further enhance scavenging rates (Miller and Wang, 1978).

5 Example of a vertical profile through the warm sector cloud

A vertical profile through the main part of the warm sector cloud was made in the location described in Fig. 1 (lower left hand black segment). The results are presented in Figs. 8 and 9. In portions of the cloud that were warmer than freezing much lower levels of rBC were found, even though the water content of the warm cloud was similar to the ice cloud (Fig. 8, middle). Examination of CO and ozone in the lower regions of the clouds (Fig. 8, bottom) indicates generally similar airmass trace gas characteristics in the lower part of the warm sector cloud, so the observed differences in rBC could be due to differences in scavenging history in the parts of the warm sector cloud that contained ice compared to the parts that were liquid. However, this portion of the cloud also contained a substantial amount of condensed water as drizzle and rain, residuals of which may be collected less efficiently by the CVI.

IN concentrations were measured at CFDC chamber temperatures between −30 and −33 °C, representing temperatures just above the top of the profile and are compared with 2DC concentrations in Fig. 9. IN concentrations agreed well with observed 2DC concentrations from the top of the profile to about 5.5 km altitude, representing a temperature range of −22 to −6.4 °C, even though the temperatures in the CFDC were significantly colder. These results contrast with the measurements made (at slightly colder ambient temperatures) in the horizontal pass described in the previous section, where the concentrations of IN were greater than the 2DC ice concentration when the temperature in the chamber was only modestly colder than ambient. Nevertheless, the

ACPD
11, 567–595, 2011

results are suggestive of heterogeneous freezing occurring at colder temperatures in the mid or upper cloud regions (in this example between −24 to −33 °C) supplying ice crystals to warmer temperatures (i.e. for this profile −22 to −6.4 °C) in this region of the storm.

6 Aerosol and IN compositions in the CVI residual particles

Since additional particles are added to the ice crystals after nucleation, and the actual IN are a small subset of these, transmission electron microscopy with energy-dispersive X-ray spectroscopy (EDS) was performed on two different types of collected particles: CVI residual particles, and the subset of those acting as IN in the CFDC. Scanning electron microscopy (SEM) with EDS was performed on the CVI residual particles only. The TEM samples were collected by impaction on grids with carbon support films and the effective smallest size was approximately 50 nm (although features as small as 20 nm can be resolved under the analytical conditions). The SEM analysis was both by manual techniques (for which 50 nm can be observed but the collection efficiency drops off rapidly below 100 nm) and by automated techniques with a lower size limit of 200 nm.

Both CVI and CFDC samples contained large fractions of particles that appear to be amorphous organic material and most of these particles have many small (20–50 nm) inclusions. An example image of one typical particle is provided in Fig. 10. Similar particles without inclusions contain only carbon and oxygen as detected by EDS (hydrogen cannot be done by EDS and nitrogen is best done by other methods). Some particles on the CVI grids were straddling holes in the holey carbon support film, so the presence of carbon and oxygen in those cases was not from the film. In the CVI samples, some of the amorphous, irregularly shaped particles contain crystals of compounds for which the EDS spectra only indicate carbon and oxygen and therefore appear also to be organic compounds. However, the majority of organic particles with inclusions in both the CVI and CFDC samples (comprising ~25% of the 50 residual IN analyzed) contain

ACPD
11, 567–595, 2011

potassium and various combinations of sodium, magnesium, calcium, potassium, sulfur and chlorine which is probably a reflection of the combined composition of the inclusions. The combination of organic material with potassium and these other elements suggests biomass burning as a source. These organic particles were the most abundant and were the likely source of the total particle number concentration seen from the SP2, which was at least an order of magnitude higher in concentration that then rBC concentration (Fig. 7). The most common particle type that would likely be sampled as rBC appears to be structureless char, suggesting incomplete combustion (as smoldering conditions would also favor organic particles). Distinct carbon spherules (i.e., soot) were not found in the samples. However, inclusions of small carbon spherule clusters (e.g., 20–30 nm) in the organic particles cannot be ruled out without new higher resolution TEM analysis. Twohy et al. (2010) found ice concentrations in orographic clouds over the Western United States were correlated with upstream concentrations of biomass burning aerosol particles.

Other particles present, although in lesser abundance than the organic particles, in both the CVI and as components of a few CFDC samples are ammonium sulfate and, as mentioned, char. Ammonium sulfate particles are present both as separate from organic particles and as inclusions. Of the 4108 CVI-sampled particles that were analyzed (with a minimum of 1000 particles per sample), only 28 of them were primarily silica and 42 were aluminosilicates (such as clay) with a median diameter of 0.9 µm for the 70 particles. Alumina silicates, a common class of IN, were not observed in the CFDC TEM samples (with a much smaller number of particles analyzed). Silicates may have been present in the CFDC samples as suggested by up to 40% of particles analyzed containing primary elements of silicon and oxygen, but interference problems with Si for the CFDC grid made it difficult to compare this element for CVI and CFDC particles. Small silica particles may be present as inclusions in a minority of the organic particles in the CVI samples.

ACPD
11, 567–595, 2011

Using the TEM results only (50 particles per sample) the EDS results suggest that in a comparison between the total CVI and CVI/IN samples, the clearly biomass-type IN samples have included particles that tend to be higher in calcium, with a median size of 0.7 µm. Both calcite and gypsum have been observed to have ice nucleating ability in at least one study (Roberts and Hallett, 1968). In the overlapping but larger size fraction represented by an automated SEM sample from this time period, 53% of the CVI particles by number have detectable calcium. Also, 70% of the CVI particles in the SEM results have detectable potassium, a very high percentage that supports a dominant biomass burning origin for the aerosol (77% of the analyzed SEM particles are between 200–1000 nm diameter). The same set of elements (Na, Mg, K, Ca, S, Cl) are in the majority of the SEM analyzed CVI particles, particles that appear to be the same as the organic particles in the TEM samples, but in the SEM the presence of inclusions cannot be observed.

While some studies have inferred that organic coatings are detrimental to ice nucleation, Koehler et al. (2010) have shown that this is not the case for secondary organic aerosol coatings in the mixed phase cloud regime warmer than −36 °C. It is also of note that based on the SP-2 data, several rBC particles were present per ice crystal. However, rBC in the form of soot was not clearly identified in the particles that actually formed ice inside the CFDC; instead the particles appeared to have a biomass burning source and were of a type that would be detected as rBC based upon their multi-component nature.

7 Summary

Few concurrent measurements of ice particle concentrations and measurements of IN from within ice crystals are available. The evidence presented here suggests that large ice crystals, such as we observed in the midlevels of an extratropical storm, release multiple aerosol particles upon evaporation in the CVI. However, the subset of these aerosols that are IN correspond with the number of ice crystals measured in the cloud

ACPD
11, 567–595, 2011

at storm midlevels when the CFDC was processing at similar temperatures. At this location, conditions were cold enough for heterogeneous freezing to be significant. The fact that the number of ice crystals agrees with the number of IN suggests that each ice crystal had formed on approximately one IN. This indicates the likely importance of primary heterogeneous freezing as the origin of the ice particles in the mid levels of the storm. However at warmer temperatures (in this case between −22 and −6.4 °C), the ice particle concentrations were similar to the IN concentrations processed at colder temperatures. Our observations suggest a conceptual model for ice formation in these warm sector clouds where heterogeneous freezing supplies large numbers of ice crystals to the mid or upper regions of the storm and these particles continue to grow as they descend to warmer temperatures maintaining concentrations similar to those at colder temperatures. Satellite observations of this storm suggest that the highest tops of the clouds were cold enough that homogeneous freezing might also be important. (However, we did not sample at these temperatures.) Had homogeneous freezing contributed significantly to the ice concentrations in the regions we studied, we would expect numbers at storm midlevels to be higher than expected from heterogeneous freezing alone, which was not observed. Ice multiplication, via Hallett-Mossop rime splintering appears unlikely in this case, due to the near absence of liquid water (and graupel, not shown) in temperatures where rime splintering occurs (Fig. 9). These conclusions cloud be further examined through numerical simulations.

While there was of order a single IN associated with each ice particle in the mid regions of the clouds, about 5 to 10 rBC particles were found for each IN or ice particle (Fig. 7). This appears consistent with the suggestion by Baumgardner et al. (2008) that inertial scavenging (or other non-nucleation scavenging processes) is more important than nucleation scavenging in contributing to the average number of rBC particles associated with each ice crystal. Miller and Wang (1989), based on a review of field observations, suggest that falling ice crystals may remove up to fifty times more efficiently than the equivalent liquid water content of falling raindrops.

ACPD
11, 567–595, 2011

Our measurements and observations suggest that biomass burning derived organic and refractory black carbon from East Asia are incorporated into the ice phase of Pacific extratropical storms. While these particles acted as IN in high enough concentrations to explain the observed ice concentrations in the storm through heterogeneous nucleation, the primary route for the rBC (and other particle) incorporation into the ice phase appears to be through non nucleation scavenging. Based upon the chemical analyses on the IN that has been done to-date, particles that served as IN were found to be slightly enhanced in calcium, but were otherwise similar to other residual particles that were found in the sample. Chemical and morphological analysis of the residual and IN particles collected during this storm and from other PACDEX cases continues and should provide more details on the properties of this important class of aerosol.

Acknowledgements. The National Center for Atmospheric Research is supported by the National Science Foundation. This work was also supported by NSF Grants ATM-0611936 (DeMott), ATM-0612605 (Baumgardner), ATM-0612605 (Twohy), and ATM-076671 (Anderson). Additional support was provided by NASA grant NNX08AH57G (Twohy). Comments on the manuscript by J. Jensen and L. Emmons are appreciated. The authors gratefully acknowledge the NOAA Air Resources Laboratory (ARL) for the provision of the HYSPLIT transport and dispersion model used in this publication.

References

Ackerman, A. S., Toon, O. B., Stevens, D. E., Heymsfield, A. J., Ramanathan, V., and Welton, E. J.: Reduction of tropical cloudiness by soot, Science, 288, 1042–1047, 2000.

Anderson, T. L. and Twohy, C. H.: Collection and exclusion of large cloud elements with a counterflow virtual impactor, Twelfth Annual Conference, Oak Brook, Illinois, American Association for Aerosol Research, 36, 1993.

Baumgardner, D., Subramanian, R., Twohy, C., Stith, J. and Kok, G.: Scavenging of black carbon by ice crystals over the Northern Pacific, Geophys. Res. Lett., 35, L22815, doi:10.1029/2008GL035764, 2008.

ACPD
11, 567–595, 2011

Chen, J.-P. and Crutzen, P. J.: Solute effects on the evaporation of ice particles, J. Geophys. Res., 99, D9, 18847–18859, doi:10.1029/94JD01346, 1994.
Cozic, J., Mertes, S., Verheggen, B., Cziczo, D. J., Gallavardin, S. J., Walter, S., Baltensperger, U., and Weingartner, E.: Black carbon enrichment in atmospheric ice particle residuals observed in lower tropospheric mixed phase clouds, J. Geophys. Res., 113, D15209, doi:10.1029/2007/JD009266, 2008.
DeMott, P. J., Prenni, A. J., Liu, X., Kreidenweis, S. M., Petters, M. D., Twohy, C. H., Richardson, M. S., Eidhammer, T., and Rogers, D. C.: Predicting global atmospheric ice nuclei distributions and their impacts on climate, P. Natl. Acad. Sci. USA, 107, 11217–11222, 2010.
Draxler, R. R. and Rolph, G. D.: HYSPLIT (HYbrid Single-Particle Lagrangian Integrated Trajectory) Model access via NOAA ARL READY Website, http://ready.arl.noaa.gov/HYSPLIT.php, last access: 26 March 2008, NOAA Air Resources Laboratory, Silver Spring, MD, USA, 2010.
Eidhammer, T., DeMott, P. J., Prenni, A. J., Petters, M. D., Twohy, C. H., Rogers, D. C., Stith, J., Heymsfield, A., Wang, Z., Pratt, K. A., Prather, K. A., Murphy, S. M., Seinfeld, J. H., Subramanian, R., and Dreidenweis, M.: Ice initiation by aerosol particles: measured and predicted ice nuclei concentrations versus measured ice crystal concentrations in an orographic wave cloud, J. Atmos. Sci., 67, 2417–2436, doi:10.1175/2010JAS3266.1, 2010.
Hadley, O. L., Ramanathan, V., Carmichael, G. R., Tang, Y., Corrigan, C. E., Roberts, G. C., and Mauger, G. S.: Trans-Pacific transport of black carbon and fine aerosols (D<2.5 µm) into North America, J. Geophys. Res., 112, D05309, doi:10.1029/2006JD007632, 2007.
Jacobson, M.: Effects of externally-through-internally-mixed soot inclusions within clouds and precipitation on global climate, J. Phys. Chem. A, 110, 6860–6873, 2006.
Jensen, E. J., Lawson, P., Baker, B., Pilson, B., Mo, Q., Heymsfield, A. J., Bansemer, A., Bui, T. P., McGill, M., Hlavka, D., Heymsfield, G., Platnick, S., Arnold, G. T., and Tanelli, S.: On the importance of small ice crystals in tropical anvil cirrus, Atmos. Chem. Phys., 9, 5519–5537, doi:10.5194/acp-9-5519-2009, 2009.
Koehler, K. A., Kreidenweis, S. M., DeMott, P. J., Petters, M. D., Prenni, A. J., and Möhler, O.: Laboratory investigations of the impact of mineral dust aerosol on cold cloud formation, Atmos. Chem. Phys., 10, 11955–11968, doi:10.5194/acp-10-11955-2010, 2010.
Menon, S., Hansen, J., Nazarenko, L., and Luo, Y.: Climate effects of black carbon aerosols in China and India, Science, 297, 2250–2253, 2002.
Miller, N. L. and Wang, P. K.: Theoretical determination of the efficiency of aerosol particle

ACPD
11, 567–595, 2011

collection by falling columnar ice crystals, J. Atmos. Sci., 46, 1656–1663, 1989.
Pilch, M. and Erdman, C. A.: Use of breakup time data and velocity history data to predict the maximum size of stable fragments for acceleration-induced breakup of a liquid drop, Int. J. Multiphas. Flow, 13, 741–757, 1987.
Prenni, A. J., Petters, M. D., Dreidenweis, S. M., Heald, C. L., Martin, S. T., Artaxo, P., Garland, R. M., Wollny, A. G. and Pöschl, U.: Relative roles of biogenic emissions and Saharan dust as ice nuclei in the Amazon Basin, Nat. Geosci., 2, 402–405, 2009.
Ramanathan, V. and Carmichael, G. C.: Global and regional climate changes due to black carbon, Nat. Geosci., 1, 221–227, doi:10.1038/ngeo156, 2008.
Roberts, P. and Hallett, J.: A laboratory study of the ice nucleating properties of some mineral particulates, Q. J. Roy. Meteor. Soc., 94, 25–34, 1968.
Schwarzenböck, A. and Heintzenberg, J.: Cut size minimization and cloud element break-up in a ground-based CVI, J. Aerosol Sci., 31, 477–489, 2000.
Stith, J. L., Ramanathan, V., Cooper, W. A., Roberts, G. C., DeMott, P. J., Carmichael, G., Hatch, C. D., Adhikary, B., Twohy, C. H., Rogers, D. C., Baumgardner, D., Prenni, A. J., Campos, T., Gao, R.-S., Anderson J., and Feng, Y.: An overview of aircraft observations from the Pacific Dust Experiment campaign, J. Geophys. Res., 114, D05207, doi:10.1029/2008JD010924, 2009.
Tarnogrodzki, A.: Theoretical prediction of the critical Weber number, Int. J. Multiphas. Flow, 19, 329–336, 1993.
Twohy, C. H., Strapp, J. W., and Wendisch, M.: Performance of a counterflow virtual impactor in the NASA Icing Research Tunnel, J. Atmos. Ocean. Tech., 20, 781–790. 2003.
Twohy, C. H., DeMott, P. J., Pratt, K. A., Subramanian, R., Kok, G. L., Murphy, S. M., Lersch, T., Heymsfield, A. J., Wang, Z., Prather, K. A., and Seinfeld, J. H.: Relationships of biomass burning aerosols to ice in orographic wave clouds, J. Atmos. Sci, 67, 2437–2450, doi:10.1175/2010JAS3310.1, 2010.
Weber, R. J., Clarke, A. D., Litchy, M., Li, J., Kok, G., Schillawski, R. D., and McMurry, P. H.: Spurious aerosol measurements when sampling from aircraft in the vicinity of clouds, J. Geophys. Res., 103, D21, 28337–28346, 1998.

ACPD
11, 567–595, 2011

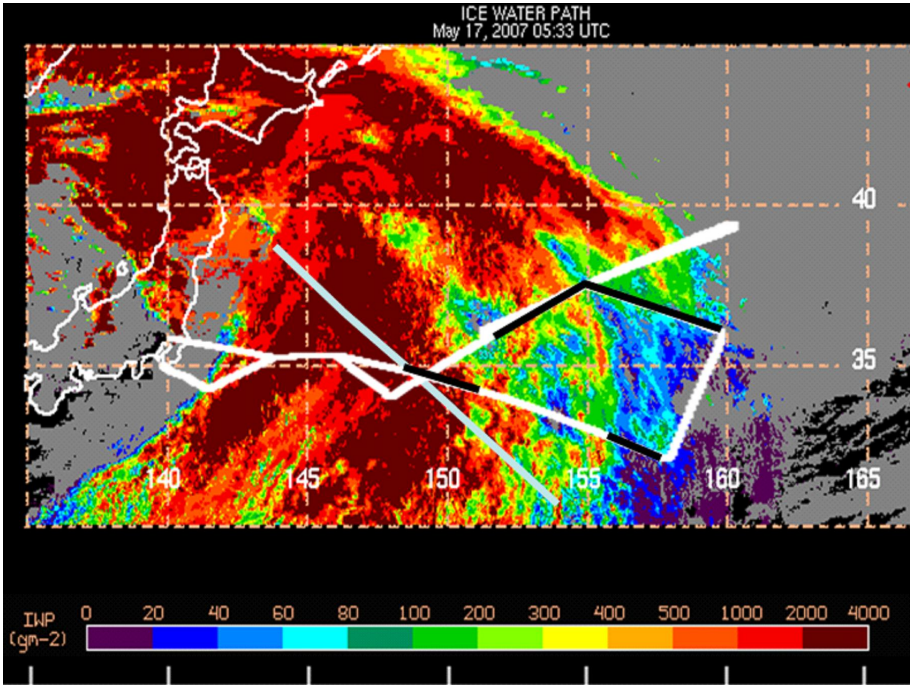

Fig. 1. Flight track of the G-V (white line) overlaid on the ice water path satellite measurements at 05:33 UT. The light blue line represents the approximate location of the near-surface warm front, based on an encounter with it at 08:19 UT at 2.1 km altitude. The black segments refer to sampling periods displayed in Figs. 5, 6, and 7 (top black line), Fig. 2 (lower right black segment), and Figs. 8 and 9 (lower left black segment). Image courtesy of NASA Langley Research Center.

ACPD
11, 567–595, 2011

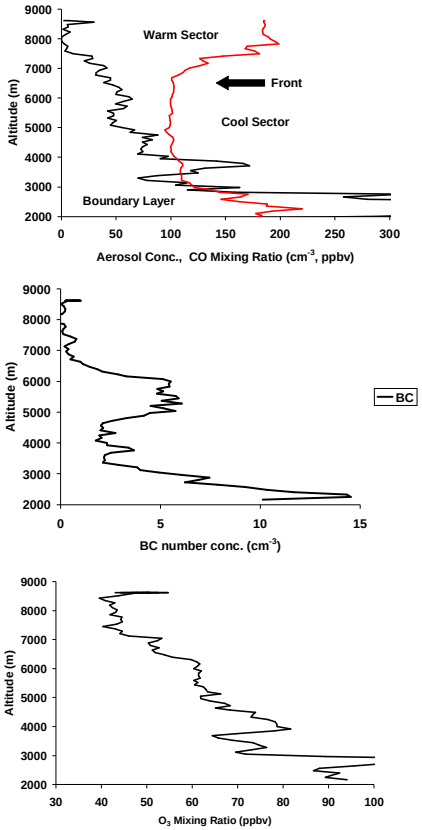

Fig. 2. Vertical profile of aerosol number concentration 0.1 to 1.0 μm in size and CO (top figure). (The lower curve for aerosol is cutoff at 300 cm^{-3}, but was over 500 cm^{-3} at the bottom of the profile). Number concentration of rBC particles (middle figure) and ozone mixing ratio (lower figure). The location for the profile is indicated in the lower right hand dark track in Fig. 1. The location of the warm frontal surface aloft and the different airmass characteristics are indicated in the top figure.

ACPD
11, 567–595, 2011

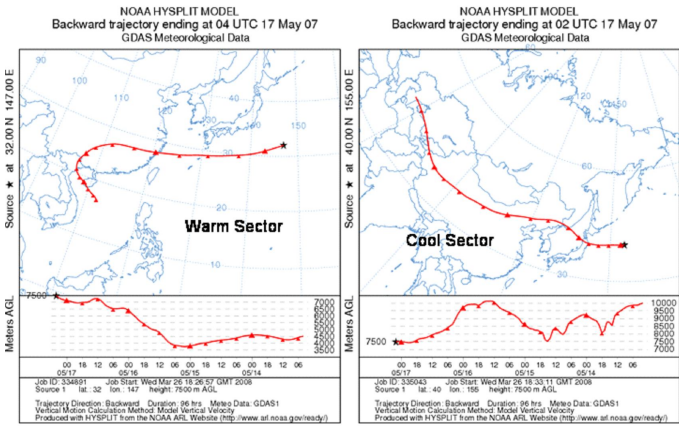

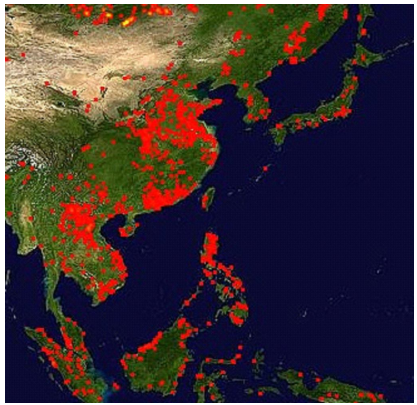

Fig. 3. (Top) NOAA HYSPLIT back trajectories for warm sector air and cool sector air. (Bottom) MODIS fire locations for 11 May through 20 May 2010, (credit: NASA/GSFC, MODIS Rapid Response).

ACPD
11, 567–595, 2011

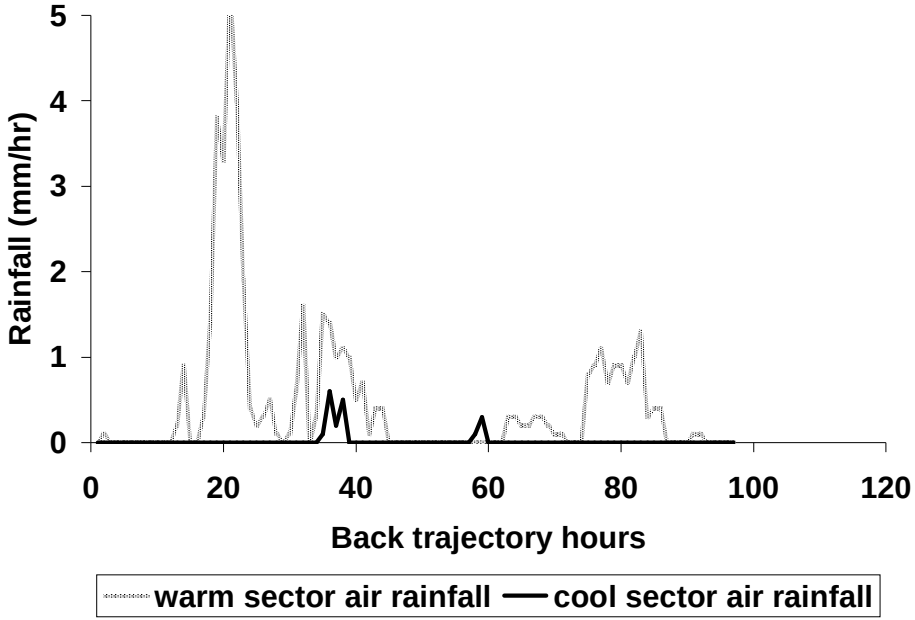

Fig. 4. NOAA HYSPLIT rainfall history for the back trajectories indicated in Fig. 3.

ACPD
11, 567–595, 2011

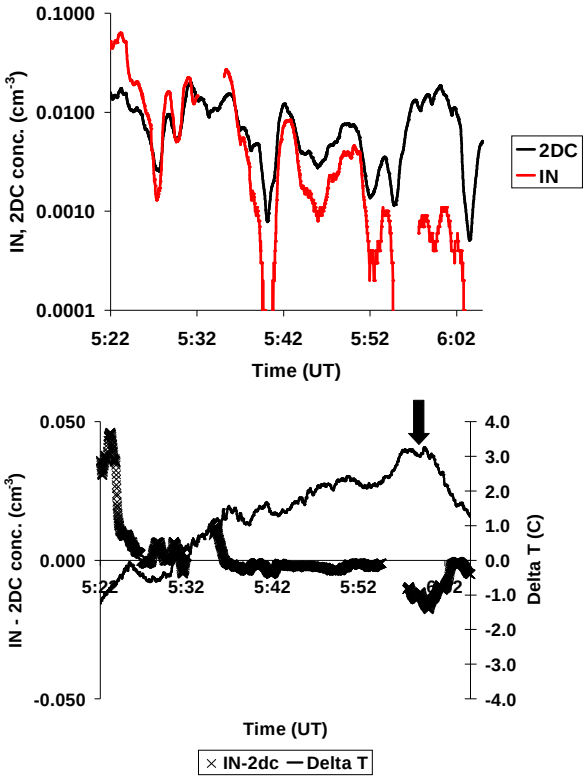

Fig. 5. (Top) Concentrations of ice particles measured by the 2DC and the simultaneous IN concentrations in the particle residue between 05:22 and 06:05 UT, which corresponds to the long black track segment in Fig. 1 (1 Hz values smoothed by 60 s running mean). (Bottom) The difference between the IN concentrations and the 2DC concentrations and the corresponding temperature difference between the CFDC chamber and the ambient temperature (1 Hz values). This pass was made at an altitude of 8.5 km. The chamber temperature at 05:42 UT was −25 °C. The location of the warm front is given by the arrow.

ACPD
11, 567–595, 2011

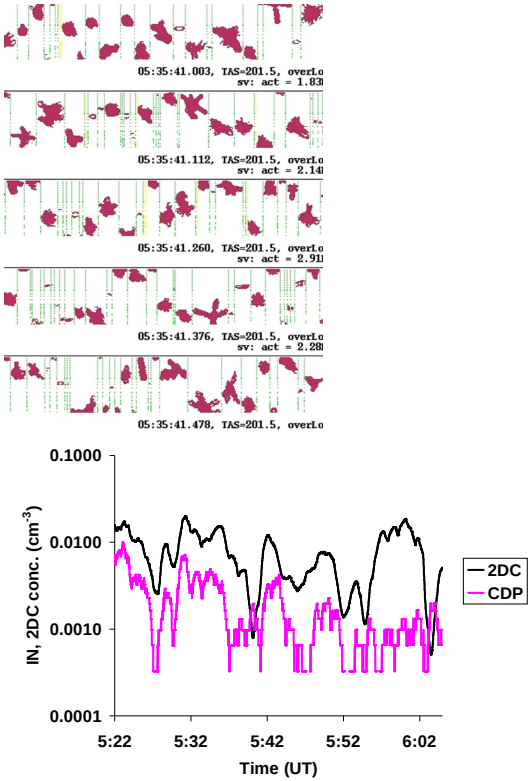

Fig. 6. (Top) Examples of 2DC imagery during the pass depicted in Fig. 5 at 05:35:41 UT. The vertical dimension of the images is 1.6 mm. (Bottom) As in Fig. 5 (top), except for 2DC and CDP measurements.

ACPD
11, 567–595, 2011

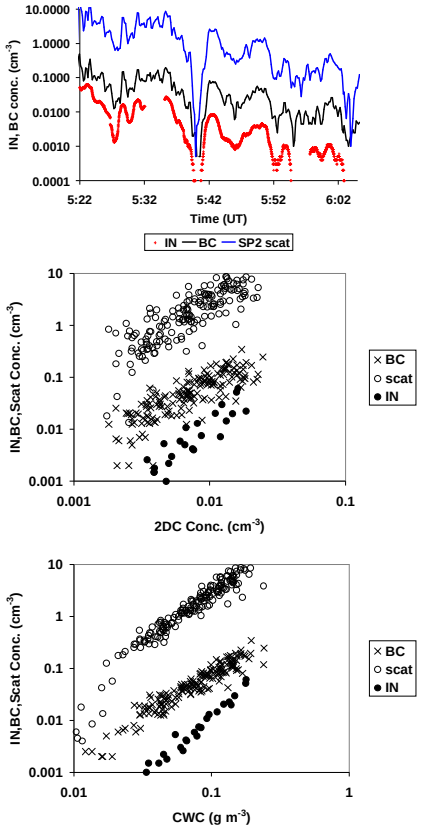

Fig. 7. Number concentrations of total SP2 scattering, rBC and IN concentrations in CVI residue versus time (top), 2DC concentration (middle) and CVI condensed water content (bottom) for the same time period. IN data in top plot are as in Fig. 5 and are 60 s averages in bottom and middle plots.

ACPD
11, 567–595, 2011

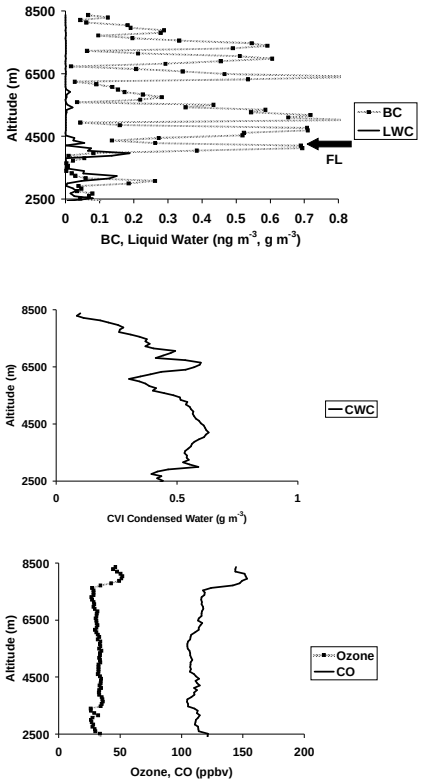

Fig. 8. Profile of warm sector cloud just above the front, showing the rBC number concentration and liquid water concentration (top) and the total water content concentration (middle) and the CO and Ozone mixing ratios (bottom). The location of the profile is in the lower left hand dark track in Fig. 1. The freezing level was at 4.2 km altitude (arrow).

ACPD
11, 567–595, 2011

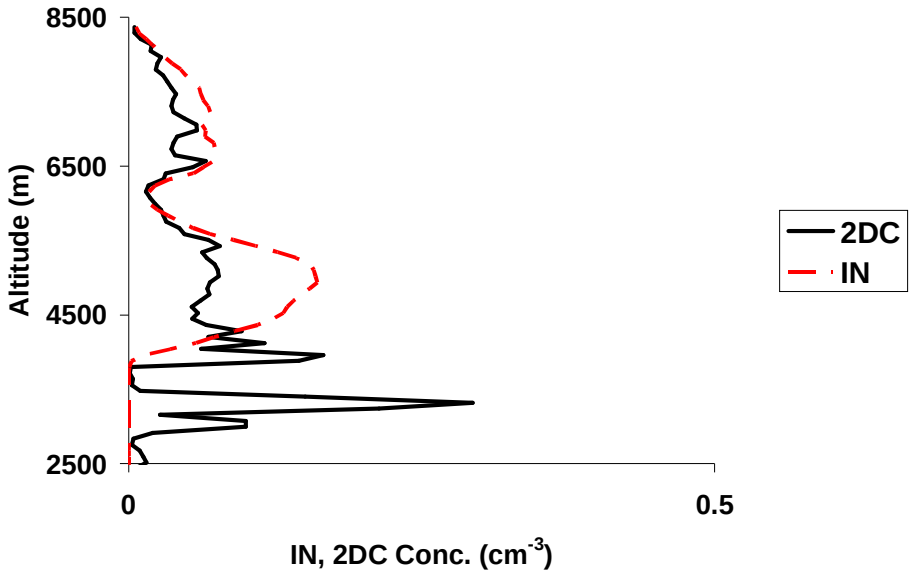

Fig. 9. Vertical profile of IN and 2DC concentrations during the vertical profile in Fig. 8. The CFDC was operated at a temperature between −30 and −33 °C.

ACPD
11, 567–595, 2011

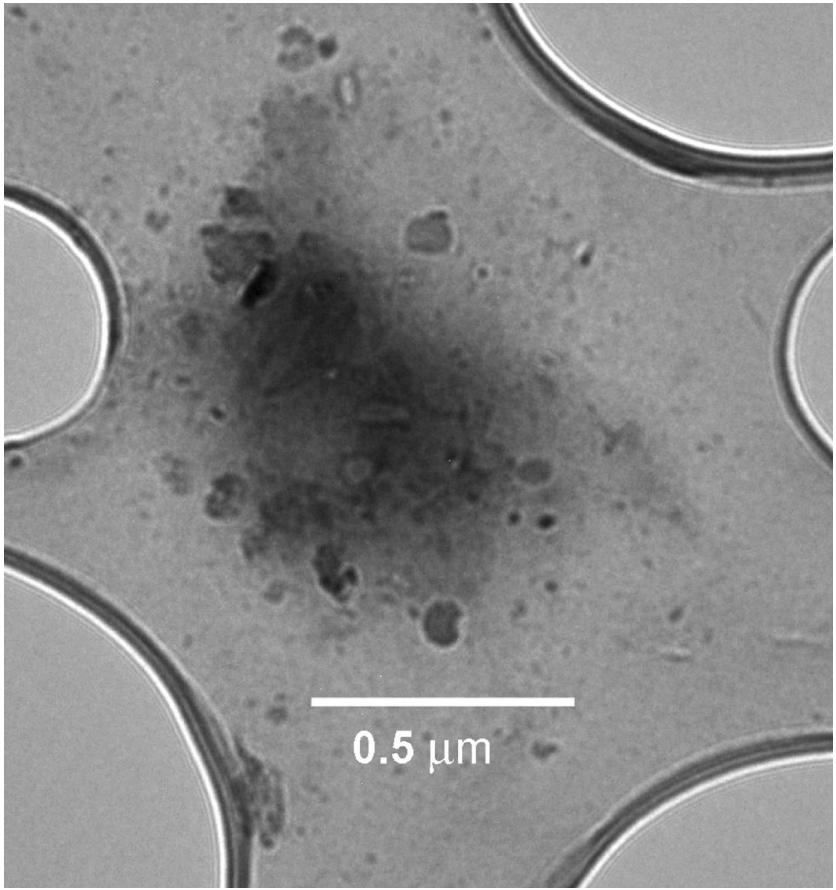

Fig. 10. TEM image of one of the residual particles from the CVI, showing the presence of inclusions in amorphous organic material. See text for more explanation.

ACPD
11, 567–595, 2011